Hydraulic resistance of artificial vegetation patches in aligned and staggered configurations

MARIO SAVIO, *VIACQUA SpA, Vicenza, Italy*

Email: ing.saviomario@gmail.com

DAVIDE VETTORI (IAHR Member), Research Fellow, *Department of Environment, Land and Infrastructure Engineering, Politecnico di Torino, Torino, Italy*

Email: davide.vettori@polito.it (author for correspondence)

HAMISH BIGGS, Ecohydraulics Scientist, *National Institute of Water & Atmospheric Research Ltd, Christchurch, New Zealand*

Email: Hamish.Biggs@niwa.co.nz

ANDREA ZAMPIRON, Research Fellow, *School of Engineering, University of Aberdeen, Aberdeen, United Kingdom*

Email: andrea.zampiron@abdn.ac.uk

STUART CAMERON, Senior Research Fellow, *School of Engineering, University of Aberdeen, Aberdeen, United Kingdom*

Email: s.cameron@abdn.ac.uk

MARK STEWART, Lecturer, *School of Engineering, University of Aberdeen, Aberdeen, United Kingdom*

Email: mstewart@abdn.ac.uk

CHRIS SOULSBY, Professor, *Northern Rivers Institute, School of Geosciences, University of Aberdeen, Aberdeen, United Kingdom*

Email: c.soulsby@abdn.ac.uk

VLADIMIR NIKORA (IAHR Member), Professor, *School of Engineering, University of Aberdeen, Aberdeen, United Kingdom*

Email: v.nikora@abdn.ac.uk

Running Head (i.e. the text that appears in the top margin of the published page): Hydraulic resistance of patchy-vegetated channels.

Hydraulic resistance of artificial vegetation patches in aligned and staggered configurations

ABSTRACT

The paper reports the results of laboratory experiments to investigate the effect of vegetation patch mosaics on hydraulic resistance. Experiments were run for seven levels of vegetation coverage with square patches of flexible plastic grass in aligned and staggered configurations and a wide range of hydraulic conditions. Hydraulic resistance was substantially higher for staggered than aligned configurations, particularly for intermediate ranges of vegetation coverage. The results indicate that hydraulic resistance differs between regimes of isolated roughness flow, wake interference flow, and skimming flow. Two types of models are proposed to predict hydraulic resistance (i.e., Manning's coefficient n) for aligned and staggered configurations, one as a function of the nondimensional spatially-averaged hydraulic radius and another as a function of relative submergence and surface area blockage factor. To account for the effects of vegetation patch alignment, an additional factor α is introduced. This work provides comprehensive datasets and models that can be used to improve the prediction of hydraulic resistance in open-channel flows with vegetation patches.

Keywords: Ecohydraulics; Environmental fluid mechanics; Flow-biota interactions; Hydraulic resistance; Vegetated flows

1. Introduction

Submerged vegetation is an important component of aquatic environments and is prevalent in many lowland rivers, streams, and canals globally. It plays significant roles in aquatic ecosystems, including serving as a habitat for invertebrates and fish (e.g. Figueiredo et al., 2015). Aquatic vegetation commonly forms patch mosaics on stream beds that create heterogeneous hydraulic habitat conditions, raise water levels, and influence nutrient dynamics (e.g. Cornacchia et al., 2019). At low-to-medium biomass levels, vegetation is usually considered to be beneficial for aquatic environments. However, at high biomass levels it can cause modification of fluvial processes, such as enhancing deposition of fine sediments and increasing river levels (e.g. Biggs et al., 2021; Butcher, 1933; Gurnell et al., 2006). These processes can lead to undesired effects, such as agricultural land becoming waterlogged or channels overtopping their banks.

Engineers and river managers are tasked with maintaining flow conveyance and predicting water levels for a range of anticipated discharges. For unvegetated rivers with flow depth much larger than roughness height, resistance coefficients (such as Manning's n) are assumed to be invariant of discharge (within a typical range of flows) and can often be

estimated by comparison of a site with published data or relationships (e.g. Barnes, 1967; Chow, 1959; Hicks & Mason, 1998), or by summation methods (e.g. Arcement & Schneider, 1989; Cowan, 1956). For vegetated rivers the situation is more complex, since vegetation drag force (and thus hydraulic resistance) is a function of many factors such as vegetation morphology, plant biomechanics, spatial distributions and relative submergence (e.g. Albayrak et al., 2012; Luhar & Nepf, 2011; Siniscalchi et al., 2012; Siniscalchi & Nikora, 2012). While detailed studies of these relationships are commendable, the quantification of vegetation parameters for practical hydraulic applications is problematic, as many of them constantly change over time due to natural processes of growth and removal. To address this issue, practical methods to estimate hydraulic resistance based on routine field measurements (or observations) of aquatic vegetation are required. Appropriate field techniques are quickly emerging, e.g., spatial distributions of in-stream vegetation can be quantified with remote sensing techniques in 2D (e.g. Biggs et al., 2018; Husson et al., 2014), or 3D when coupled with ground truth measurements (Biggs, 2020).

Early progress on estimating the hydraulic resistance of vegetated channels was made by Kouwen and collaborators (Kouwen et al., 1969; Kouwen & Unny, 1973). Since then most works have been dedicated to channels covered with uniform vegetation, with only a few exceptions wherein vegetation patch mosaics were considered (Afzalimehr et al., 2021; Nepf, 2012). Over the past 20 years, several relationships between blockage factors and hydraulic resistance coefficients for patch mosaics obtained via best-fit of field data have been proposed (Green, 2005a; V. Nikora et al., 2008). Green (2005) suggested that the vegetation contribution to Manning's n is equal to $0.0043B^x$-0.0497, where B^x is the cross-sectional blockage factor, defined as the proportion of a cross-section covered in vegetation (Green used the weighted median value of B^x across a number of cross-sections); while V. Nikora et al. (2008) found a relationship between Manning's n and the reach-averaged cross-sectional blockage factor ($B^{x,ave}$), namely $n = 0.025e^{3Bx,ave}$. Later, Luhar and Nepf (2013) performed an analysis of vegetation drag across spatial scales and, using the momentum balance, derived that $n \propto (1 - B^x)^{-3/2}$, which was tested using the data collected by Green (2005) and Nikora et al. (2008).

Due to the nature of field measurements, Green (2005) and V. Nikora et al. (2008) were unable to vary vegetation spatial configurations or overall aquatic vegetation coverage and hence assess their effects on hydraulic resistance. To assess the effect of patch patterns and provide quantitative relationships between aquatic vegetation coverage, hydraulic conditions and hydraulic resistance, a detailed flume-based study was undertaken using artificial vegetation patches. Aligned and staggered patch configurations were considered for 7 different aquatic vegetation coverages (0%, 10%, 20%, 30%, 40%, 60%, and 100%), at a range of relative submergences. The aim of this paper is to quantify the effects of regular

patch mosaic patterns (aligned and staggered) on the overall (bulk) hydraulic resistance in vegetated channels.

2. Experimental design and facility

2.1. Open channel facility

Experiments were conducted in a tilting re-circulating flume in the Fluid Mechanics Laboratory at the University of Aberdeen (Zampiron et al., 2020). The flume is 10.75 m long, 0.4 m wide, and has a maximum flow rate of 22 L s^{-1}. Flume inclination is adjusted using a screw jacking system, which supports multiple points along the flume to maintain a constant slope S. The flow rate Q is measured with an electromagnetic flow meter (MagMaster, ABB, Zurich, Switzerland) in the inflow pipe prior to the flume entrance. The accuracy of the flow meter is quoted as ± 0.15% of the measured flow rate. The flume has 10 equally spaced metal rulers glued to the glass side wall, enabling water depth to be measured along the flume with an accuracy of ± 0.5 mm. At the same cross-sections along the flume, 10 piezometer intakes are positioned on the bed centreline to measure the water surface profile with an accuracy of ± 0.5 mm. During the experiments, the entire length of the flume was covered in replica of aquatic vegetation in a range of spatial configurations and coverages. The mean (i.e. time-averaged) deflected height (h_v) of the artificial vegetation was measured using the metal rulers installed on the flume side wall.

2.2. Artificial vegetation patches

Aquatic vegetation was simulated using patches of artificial plastic grass (N. Nikora et al., 2013), which provides a useful surrogate for natural aquatic vegetation. Artificial vegetation is also more practical to use in flume experiments than natural aquatic vegetation because it will not degrade over time, thus potentially affecting the hydraulic resistance (Vettori et al., 2021). Further, the use of artificial vegetation enables a wide range of patch densities and spatial configurations to be investigated, compared to the case studies focusing on natural aquatic vegetation in rivers (e.g., Biggs et al., 2019; Nikora et al., 2008).

The artificial plastic grass used in the experiments presented herein has a mass density of 0.925 g cm^{-3}, and is comprised of individual stems 35.3 mm long, 1.19 mm wide and 0.2 mm thick. The number of stems per unit bed area is 243,600 stem m^{-2}, from which a porosity (φ) of 0.969 and a total frontal vegetation area per unit volume of 289 m^{-1} are obtained. Young's modulus of the stems was estimated as 97 GPa via tension tests on 25 stem specimens using a Hounsfield S-series bench top testing machine.

Vegetation patches were created by cutting the artificial grass into 0.1 m by 0.1 m squares, then a fabric with small loops was sewn under the polypropylene base of the vegetation patches. The bed of the flume was covered in Pressogrip®, which consists of tiny hooks approximately 0.5 mm in diameter and height (similar to Velcro). The patches were attached onto the Pressogrip® bed, thus allowing rapid changes between different scenarios of patch configuration and/or coverage. Because the artificial grass was attached to the Pressogrip® base, the measured deflected height of a patch often exceeded the length of the individual stems and was found to vary between 33 and 41 mm across the experiments. From here onwards we will refer to the artificial plastic grass as 'vegetation'.

2.3. Key parameters

For evaluating the effect of vegetation patch mosaics on hydraulic resistance we made use of blockage factors introduced in the previous studies, namely the (maximum) cross-sectional blockage factor B^{x}, the flume-averaged cross-sectional blockage factor $\mathsf{B}^{x,ave}$ (V. Nikora et al., 2008), which is equivalent to the volumetric blockage factor, and the (planform) surface area blockage factor B^{SA}, which are defined respectively as:

$$\mathsf{B}^{x} = N_y h_v b_y/(HB), \tag{1}$$

$$\mathsf{B}^{x,ave} = N_t h_v b_x b_y/(HBL), \tag{2}$$

$$\mathsf{B}^{SA} = \mathsf{B}^{x,ave} H/h_v = N_t b_x b_y/(BL), \tag{3}$$

where B and L are the flume width and length, H is the mean water depth (obtained from the readings of the 10 rulers located along the channel), b_x and b_y are the length and width of a patch (both equal to 0.1 m), h_v is the mean deflected height of a patch, and N_t and N_y are the total number of patches in the flume and number of patches across a vegetated cross section, respectively. In the vegetated cross-sections we considered the bulk area covered by the patches rather than summing the cross-sectional areas of each shoot (Green, 2005).

Although the equation for Manning's resistance coefficient $n = R_i^{2/3} S^{1/2}/U$ is widely adopted in engineering applications, the definitions of its parameters may not be straightforward. In our study, for the calculation of n we adopted the conventional approach, commonly employed in field applications, in relation to the mean velocity U and the hydraulic radius R_i, where U is defined as mean cross-sectional velocity $U = Q/A$ and $R_i = R_h$:

$$R_h = BH/(2H+B), \tag{4}$$

hence neglecting the presence of patches within the cross-sectional area $A = BH$ since patch porosity can be approximated to unity. On this account, it is worth noting that a more rigorous approach for calculating U is to consider the cross-sectional area covered by vegetation (A_v),

i.e. $U = Q/(A_f+\varphi A_v)$, where A_f is the cross-sectional area free of vegetation (so that $A = A_f+A_v$) and φ is patch porosity. However, because φ is close to unity, it may be removed from the equation, thus $A = A_f+A_v$ and $U = Q/A$.

In channels with complex geometry the hydraulic radius can also be defined accounting for the presence of patches. Here, we propose two options. First, R_i may be defined considering the patches as solid obstacles, i.e., $R_i = R_{h\text{-}veg}$:

$$R_{h\text{-}veg} = (BH\text{-}N_y h_v b_y)/(2H+B+N_{y,s}h_v), \quad (5)$$

where $N_{y,s}$ is the number of patch sides across a vegetated cross section. It is worth noting that in Eq. (5) we did not simply consider the number of patches because when $B^{SA} = 0.6$ some patch sides were contiguous to the flume side walls (see Fig. 1). Second, one may also define the spatially-averaged hydraulic radius to account for patches spatial distribution along the channel, i.e., $R_i = \langle R_h \rangle$:

$$\langle R_h \rangle = [R_h(L\text{-}N_x b_x)+R_{h\text{-}veg}N_x b_x]/L, \quad (6)$$

where N_x is the number of patch rows along the flume. It is also worth noting that $\langle R_h \rangle = R_h m+R_{h\text{-}veg}(1\text{-}m)$ is a linear function of R_h, where m is the proportion of unvegetated cross-sections along the channel (i.e. $m = 1\text{-}N_x b_x/L$). The latter expression of the hydraulic radius in nondimensional form (i.e. $\langle R_h \rangle/h_v$) is used in the data analysis that follows as an additional key parameter to assess the effect of vegetation patch mosaics on hydraulic resistance.

2.4. Experimental setup

Aquatic vegetation was arranged in regular patch mosaic patterns along the full length of the flume (Fig. 1). Five values of surface area blockage factors (B^{SA}) ranging from 0.1 to 0.6, comparable to those of natural rivers and streams (e.g. Green, 2006; V. Nikora et al., 2008), were investigated in aligned and staggered configurations. Experiments with vegetation fully covering the flume bed ($B^{SA} = 1$) and with no vegetation on the bed ($B^{SA} = 0$) were also carried out. Manning's n for the unvegetated bed was measured to be within the range 0.009 – 0.011 s $m^{-1/3}$ for $H = 0.024$ to 0.140 m. Experiments were designed so that for each value of B^{SA} approximately the same range of Reynolds number (R_e) was used. For each value of B^{SA}, two bed slopes were employed (i.e. $S = 0.001$ and 0.002) and for both bed slopes 15 to 20 runs were completed by varying the flow rate so that the mean flow depth (or water level) increased by 5 mm at a time. Uniform steady-state conditions were imposed by adjusting the weirs located at the end of the flume. The ranges of hydraulic conditions covered by the measurements are shown in Table 1.

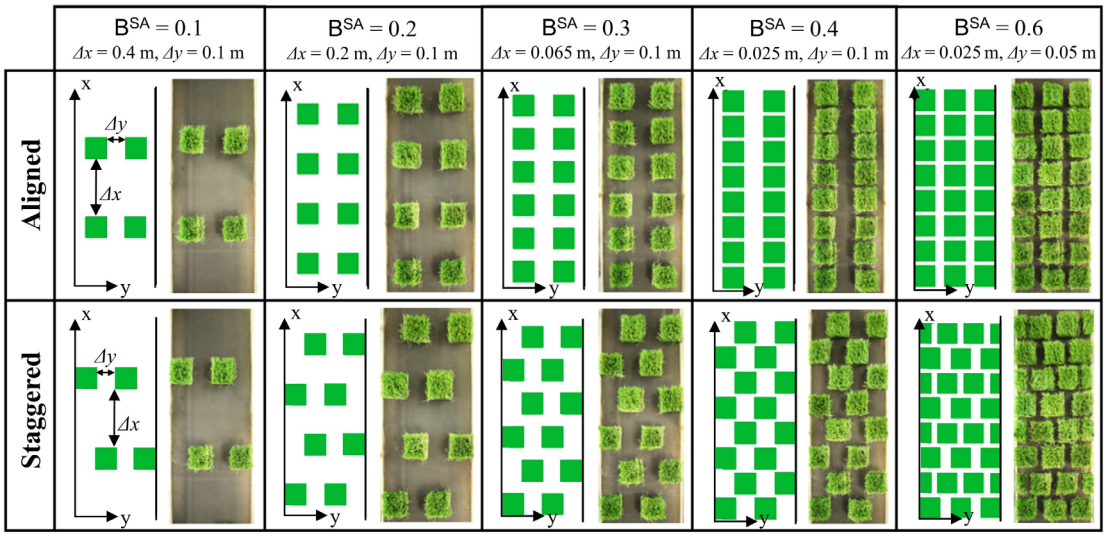

Figure 1: Schematic of patch patterns in aligned and staggered configurations.

Table 1. Ranges of hydraulic characteristics in the experiments.

B^{SA} (-)	S (-)	Q (L s^{-1})	H (m)	H/h_v (-)	B/H (-)	U (m s^{-1})	u_* (m s^{-1})	R_e (-)	F_r (-)
0	0.001-0.002	1.5-21.3	0.024-0.140	-	2.8-16.6	0.15-0.38	0.015-0.052	3600-53200	0.30-0.61
0.1	0.001-0.002	1.7-22.0	0.049-0.177	1.4-5.0	2.2-8.1	0.09-0.31	0.022-0.059	4250-55000	0.13-0.24
0.2	0.001-0.002	1.6-21.5	0.048-0.191	1.3-5.7	2.1-8.1	0.08-0.28	0.023-0.061	4000-53750	0.12-0.21
0.3	0.001-0.002	1.8-22.0	0.051-0.180	1.3-5.1	2.2-7.8	0.08-0.31	0.022-0.059	4500-55000	0.12-0.23
0.4	0.001-0.002	1.9-21.2	0.060-0.180	1.6-4.9	4.7-6.7	0.08-0.31	0.024-0.058	4750-53000	0.10-0.24
0.6	0.001-0.002	2.0-19.3	0.064-0.165	1.7-4.8	2.4-6.2	0.08-0.29	0.025-0.057	5000-48250	0.10-0.23
1	0.001-0.002	2.3-19.0	0.070-0.166	1.8-4.8	2.4-5.7	0.08-0.30	0.026-0.057	5780-49800	0.10-0.24

Note: The columns show: the surface area blockage factor B^{SA}, the bed slope S, the mean flow rate Q, the mean water depth H, the submergence ratio H/h_v, the flow aspect ratio B/H, the mean flow velocity U, the shear velocity $u_* = (gR_hS)^{1/2}$ (where g is the gravitational acceleration), the Reynolds number $R_e = UH/v$ (where v is the kinematic viscosity), and the Froude number $F_r = U/(gH)^{1/2}$.

3. Results

3.1. Hydraulic resistance of aligned patches

With aligned patches on the flume bed, hydraulic resistance (quantified with Manning's n) increased with cross sectional blockage factor (B^x) for all investigated cases (Fig. 2a). The maximum hydraulic resistance occurred for intermediate values of vegetation coverage (i.e. B^{SA} = 0.2-0.4). The resistance for the lowest and highest values of B^{SA} was generally lower. When the bed was uniformly covered by vegetation (i.e. B^{SA} = 1), hydraulic resistance was lower than when patchy vegetation was present. The effect of patch mosaic was explored further by considering the flume averaged cross-sectional blockage factor ($B^{x,ave}$) as an argument (Fig. 2b). Figure 2b shows clear separation in relationships between n and $B^{x,ave}$ for the different vegetation coverages.

Previous works based on data collected in transects of streams/rivers proposed that Manning's n can be modelled as a linear function of B^x (Champion & Tanner, 2000; Green, 2005). However, our results displayed in Fig. 2a indicate that n should not be approximated as a linear function for any case investigated, since the exponent $k1$ in the best-fit power law $n \propto (B^x)^{k1}$ varies between 0.54 and 1.03 increasing with B^{SA} ($R^2 > 0.96$). The data plotted as function of the spatially averaged blockage factor ($B^{x,ave}$, Fig. 2b) did not show any common trend, and thus must be interpreted in conjunction with information on B^{SA}.

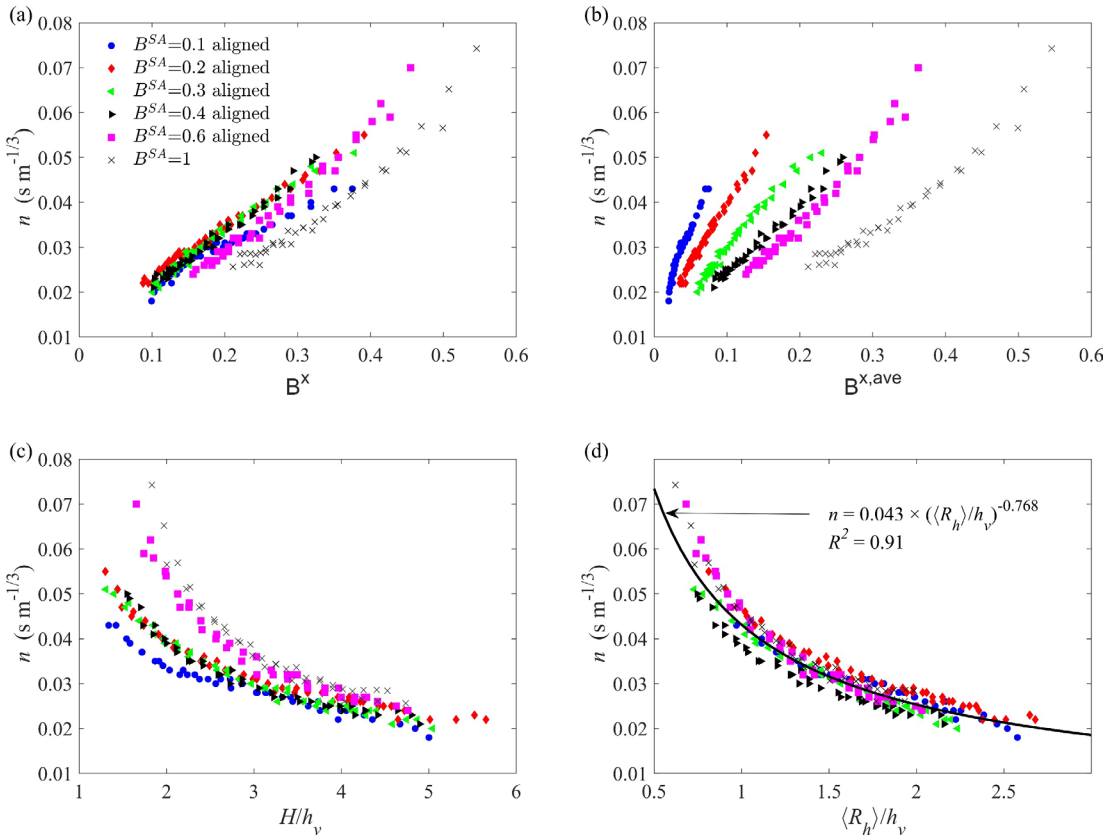

Figure 2: Manning's n for aligned vegetation patches as a function of: (a) cross sectional blockage factor; (b) flume averaged cross sectional blockage factor; (c) relative submergence; (d) nondimensional spatially-averaged hydraulic radius.

Manning's n decreased non-linearly as the relative submergence increased (Fig. 2c), in agreement with conventional hydraulics. At low relative submergence (i.e. $H/h_v < 3$), there is divergence in the relationships between Manning's n and H/h_v within the extreme values of B^{SA} (i.e. 0.1, 0.6 and 1). At higher relative submergence (i.e. $H/h_v > 3$) the data tend to converge for all values of B^{SA}. Fitting the data points for each value of B^{SA} with a relationship of the form $n \propto (H/h_v)^{k2}$, it was found that k_2 varied between -0.54 and -0.99 ($R^2 > 0.96$), decreasing with B^{SA}. The hydraulic resistance also decreased as the nondimensional spatially-averaged hydraulic radius ($\langle R_h \rangle / h_v$) increased (Fig. 2d). For $\langle R_h \rangle / h_v$, all curves for the aligned cases show a similar trend and this parameter appears to provide the best collapse, potentially indicating that $\langle R_h \rangle / h_v$ includes all major geometrical and hydrodynamic features important to the hydraulic resistance. Considering all the data for the aligned configuration the general relationship $n = 0.043(\langle R_h \rangle / h_v)^{-0.768}$ ($R^2 = 0.91$) can be obtained as best-fit. Because individual blockage factors used in previous studies are unable to provide a general relationship for n (see data stratification depending on the values of B^{SA} in Fig. 2a-c), we explored different multivariate regressions options. Based on the trends shown in Fig. 2a-c, we opted for the

form $n = f(B^{SA}, H/h_v)$ and identified the best-fit for all aligned data as the relationship $n = \exp(0.437B^{SA}-2.887)\times(H/h_v)^{-0.667}$ ($R^2 = 0.92$).

It is also interesting to assess the distributions of Manning's n depending on the surface area blockage factor (B^{SA}) for different values of relative submergence (Fig. 3). At low submergences, larger B^{SA} generate higher flow resistance. As the submergence increases, this effect is less pronounced and H/h_v becomes dominant. For all cases, the increase in n from $B^{SA} = 0.4$ to 0.6 was likely due to the decrease in spanwise distance between vegetation patches and thus the increase in vegetation coverage (Fig. 1).

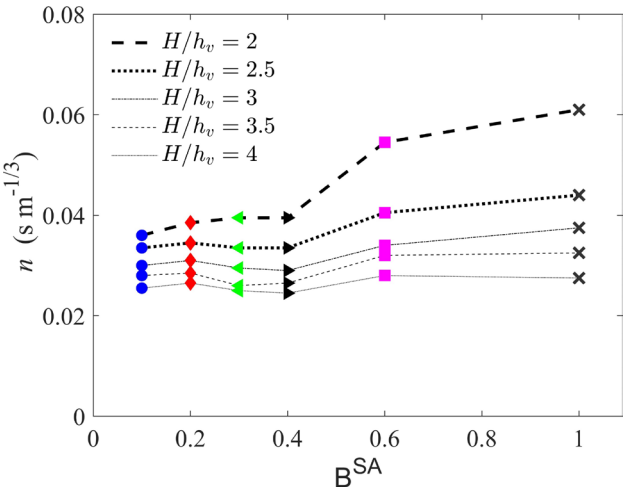

Figure 3: Manning's n for aligned vegetation patches as a function of surface area blockage factor for selected relative submergences.

3.2. Hydraulic resistance of staggered patches

Similar to aligned patches, Manning's n with staggered patches increased with cross sectional blockage factor (B^x) for all vegetation coverages tested (Fig. 4a), with the lowest values of n for the case of bed uniformly covered (i.e. $B^{SA} = 1$). The maximum hydraulic resistance occurred for intermediate values of vegetation coverage (i.e. $B^{SA} = 0.2$-0.4). This is similar to the trends observed for aligned patches (Fig. 2a), yet there is a much larger separation between intermediate and extreme values of vegetation coverage (i.e. $B^{SA} = 0.1$, 0.6-1). Again, the relationship between n and B^x should not be approximated as a linear function, but as a power law $n \propto (B^x)^{k1}$. The exponents that provide the best-fit are $k_1 = 0.57$-1.05 ($R^2 >$ 0.95), increasing with B^{SA}. Relationships between Manning's n and reach-averaged cross-sectional blockage factor $B^{x,ave}$ were also clearly separated by B^{SA} (Fig. 4b), as was found for the aligned configuration.

Manning's n decreased non-linearly as the relative submergence (Fig. 4c) and the nondimensional spatially-averaged hydraulic radius (Fig. 4d) increased. Similar to the aligned cases, the data distributions diverge as H/h_v approaches low values. For all cases, the exponent in the power law $n \propto (H/h_v)^{k2}$ was always lower than the corresponding aligned case, varying between -0.57 and -1.05 ($R^2 > 0.96$). Differently from the aligned cases, distributions of Manning's n depending on the nondimensional spatially-averaged hydraulic radius ($\langle R_h \rangle / h_v$) (Fig. 4d) display clear stratification. This is reflected by the performance of the general relationship $n = 0.054(\langle R_h \rangle / h_v)^{-0.79}$ with $R^2 = 0.68$, suggesting underlying differences in flow structure between aligned and staggered patch configurations, which will be discussed in section 4.1.

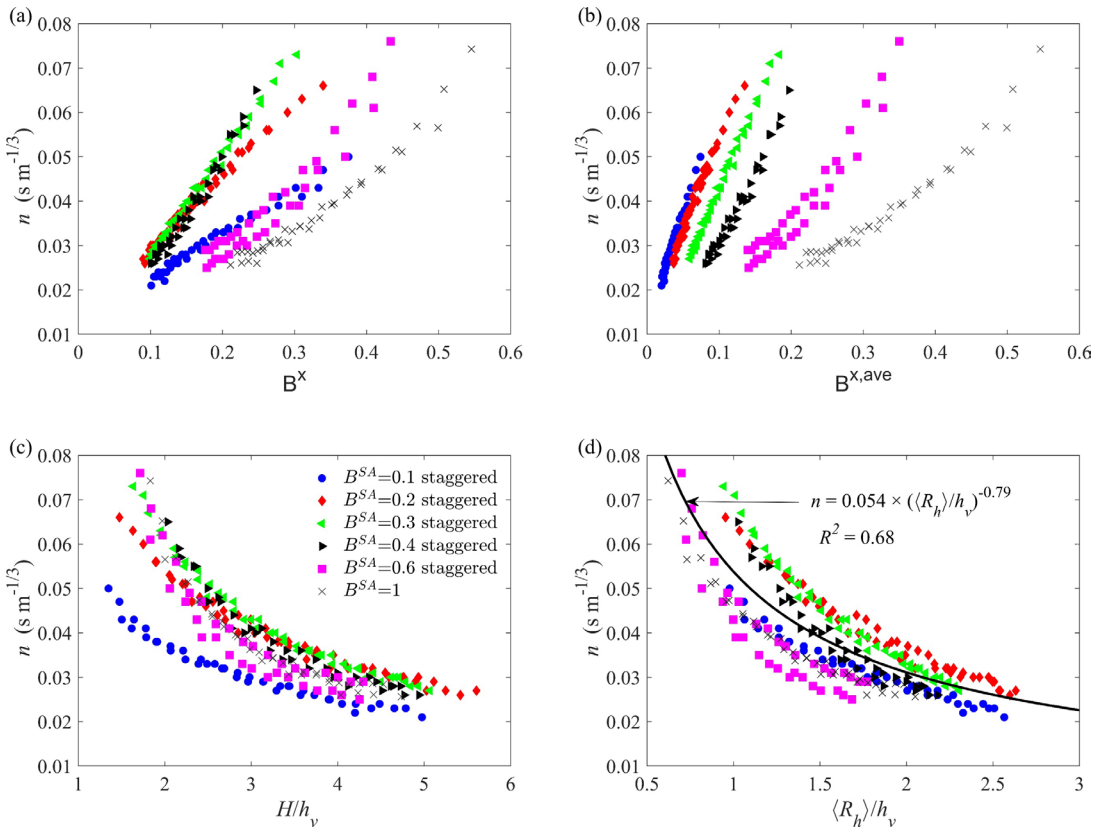

Figure 4: Manning's n for staggered vegetation patches as a function of: (a) cross sectional blockage factor; (b) flume averaged cross sectional blockage factor; (c) relative submergence; (d) nondimensional spatially-averaged hydraulic radius.

In Fig. 5, Manning's n vs the surface area blockage factor (B^{SA}) is shown for selected relative submergences (H/h_v). All distributions exhibited a similar trend regardless of the relative submergence, with the largest n at intermediate vegetation coverages (B^{SA} = 0.2 to 0.3) and a local minimum at B^{SA} = 0.6. As done for the aligned configuration, a multivariate

regression of the form $n = f(\mathrm{B}^{SA}, H/h_v)$ was explored for the staggered cases. Hence, we identified as best fit $n = \exp(0.299\mathrm{B}^{SA}-2.592)\times(H/h_v)^{-0.708}$ ($R^2 = 0.72$), with a coefficient of determination much lower than for the aligned configuration.

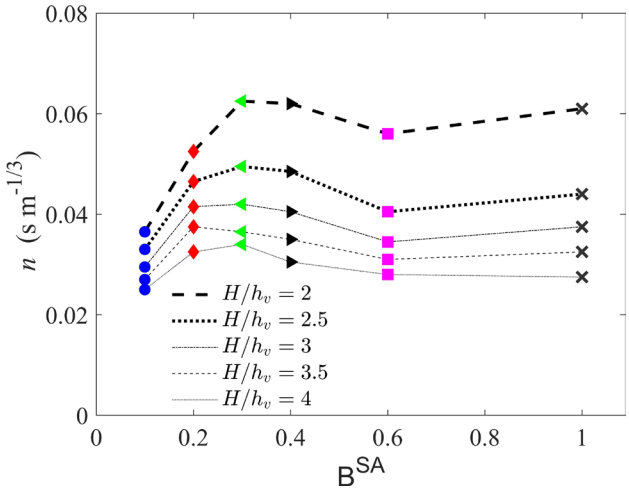

Figure 5: Manning's n for staggered vegetation patches as a function of surface area blockage factor for different relative submergences.

3.3. Comparison of hydraulic resistance between aligned and staggered patches

The previous sections indicated clear differences in hydraulic resistance for aligned and staggered patches (Figs. 2 to 5). To directly quantify this effect, we compare Manning's n from staggered and aligned configurations for the same nominal flow conditions and surface area blockage factor. Figure 6 shows the ratio of Manning's n values between staggered (n_s) and aligned configurations (n_a), which we refer to as $\alpha = n_s/n_a$ hereafter. Although data points are quite scattered, there seems to be a general trend across all cases. The staggered configuration was always characterised by a higher hydraulic resistance than the aligned configuration (i.e. $\alpha > 1$). The difference between the two patterns was enhanced at intermediate values of surface area blockage factor and at low relative submergence. The parameter α generally decreased as the relative submergence increased because a larger proportion of the flow can pass over the patches, rather than being forced through pathways between patches. The multivariate regression accounting for the effects of B^{SA} and H/h_v on α that provided the best-fit for our data was $\alpha = 1 + 4.04\mathrm{B}^{SA} - 5.83(\mathrm{B}^{SA})^2-0.09H/h_v$, with $R^2 = 0.92$.

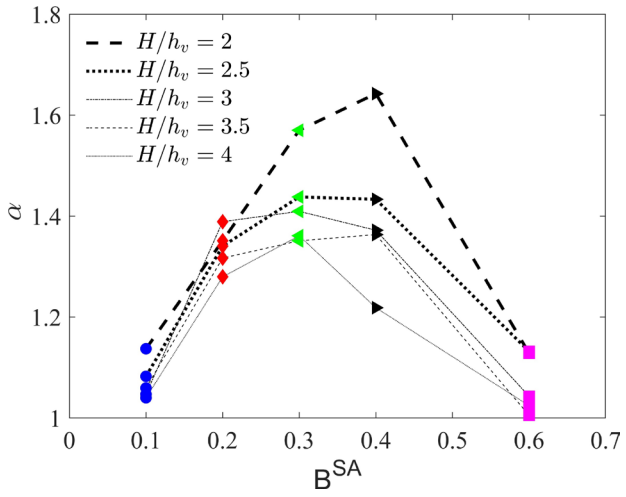

Figure 6: Ratio of Manning's n for staggered (n_s) patches to Manning's n for aligned patches (n_a) as a function of surface area blockage factor for different relative submergences.

4. Discussion

4.1. On the effects of vegetation spatial distribution

The results presented in this paper indicate that the spatial distribution of vegetation patches has important effects on hydraulic resistance. This finding agrees with Bal et al. (2011), who reported a variation in hydraulic resistance depending on the spatial pattern of plant removal in laboratory tests with live freshwater macrophytes, and Green (2006), who concluded that spatial distribution of freshwater macrophytes can affect the hydraulic resistance based on field experiments in several streams. Nevertheless, we are not aware of any study in which the effects of spatial distribution on hydraulic resistance have been rigorously quantified. Luhar and Nepf (2013) attempted to account for the spatial distribution of patches by considering a different number of patches for a given cross-sectional blockage factor, thus modelling the hydraulic resistance using a representative cross-section. However, their simplified approach had a limitation in that it neglected the effects that the patches have on the flow hydrodynamics (e.g. wakes generated by patches).

A number of works have shed light on the effects that 3-dimensional obstacles have on the flow, with the creation of three regions: (i) an upstream region wherein the flow is diverted away from the obstacle; (ii) lateral zones with increased flow velocity; and (iii) a downstream region with a wake and, when sufficient room is available, a recirculation cell (e.g. Wolfe & Nickling, 1993). Based on the classification of Morris (1955), later extended by Folkard (2011), the wake plays a crucial role in defining the flow regime in the presence of multiple obstacles. In this context, the term 'flow regime' is used to describe the flow patterns between roughness elements (e.g. between patches of vegetation in a patch mosaic/canopy).

In Figure 7, we propose a summary of the wake-patch interactions for both the aligned (Figure 7a-c) and staggered (Figure 7d-f) configurations. When the streamwise distance between patches (Δx) is sufficiently large, wakes develop downstream of patches. As Δx becomes smaller, wakes gradually disappear, and skimming flow conditions are established. For the same value of Δx, patches in staggered configuration allow more room for the wakes to develop compared to the cases with aligned patches, therefore impeding the establishment of skimming flow conditions until Δx becomes smaller.

Figure 6 shows that when B^{SA} is either very low (i.e. 0.1) or very high (i.e. 0.6) the staggered distribution increases Manning's n by 5-15%, while for intermediate values of B^{SA} it increases by over 60% compared to the aligned configuration. This is caused by the different effects that increasing vegetation coverage has on the flow features: in the aligned configuration water can flow through preferential paths even at high values of B^{SA}, while in the staggered configuration flow paths are strongly dependant on B^{SA} because patches have more complex effects on the flow.

The n coefficients for aligned patches with B^{SA} from 0.1 to 0.4 (Fig. 3) were found to be essentially unchanged. This suggests that the increase of drag due to higher vegetation coverages was counterbalanced by the transition from a wake interference flow regime (Figure 7a), where large part of the drag is generated by the patches in the form of pressure and wake drag, to a skimming flow regime (Figure 7b,c), where wakes are suppressed and flow velocity within the vegetation decreases to very low values. Note that the wake length formed by an isolated patch in the flow conditions listed in Table 1 was estimated to always exceed 0.4 m (Savio, 2017), hence impeding the establishment of an isolated roughness flow regime. For B^{SA} = 0.4 to 0.6, n increased, reflecting a decrease in spanwise distance between vegetation patches (Fig. 1), particularly at smaller submergences. For staggered patches (Fig. 5), n increased substantially from B^{SA} = 0.1 to 0.3 due to the higher vegetation coverages (Figure 7d,e). Moreover, based on the results of Savio (2017) within this range of B^{SA} we expect a transition from isolated roughness flow to wake interference flow regime. Finally, n was sharply reduced for $B^{SA} \geq 0.4$ for all submergences, likely due to the establishment of the skimming flow regime for the staggered configurations (Figure 7f). Similar threshold values for the establishment of a skimming flow regime have been reported by Lee and Soliman (1977) for wind tunnel experiments with urban canopies, Leonardi et al. (2007) for turbulent channel flow and Wolfe and Nickling (1993) for aeolian processes in sparse vegetation.

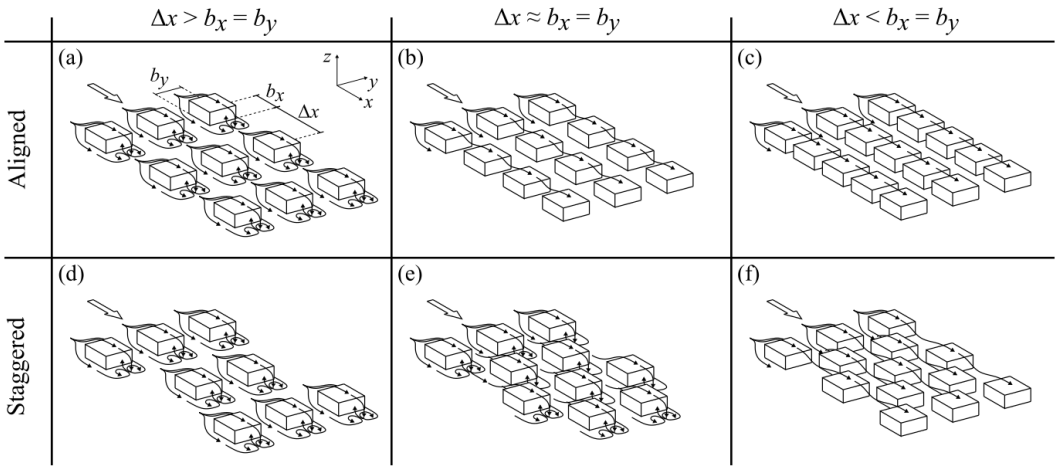

Figure 7: Schematic representation of flow patterns that develop for different patch configurations (aligned or staggered) and streamwise gaps between patches (Δx).

The values of vegetation coverage for which the difference in Manning's n between aligned and staggered configuration are most prominent (i.e. B^{SA} = 0.2-0.4, Fig. 6) are close to the "connectivity threshold" and in agreement with recent findings on connectivity in heterogeneous landscapes, such as wetlands and river deltas (e.g. Larsen et al., 2017; Wright et al., 2018). In more detail, Larsen et al. (2017) found that patch configurations in wetlands become increasingly important to define discharge when vegetation coverage threshold is close to 0.4 and at low water levels. In river deltas, Wright et al. (2018) reported that for values of coverage equal to or slightly below a threshold of 0.4-0.5 the presence of patches leads to the formation of preferential flow paths. While these environments are unlike our flume experiments both in terms of spatial scale and dimensionality of the landscape, these similarities point to some common governing mechanics.

Lastly, distributions of Manning's n shown in Fig. 5 have a very similar trend to the drag coefficient of a patch of rigid cylinders immersed in turbulent flow, both reaching the maximum for patch density (equivalent to B^{SA} in the present study) between 0.2 and 0.3 (Chang & Constantinescu, 2015; Taddei et al., 2016). This suggests that these two different settings may share some common underpinning mechanics.

4.2. On the estimate of hydraulic resistance in flows with vegetation patches

Blockage factors that have been used previously to estimate the hydraulic resistance of beds with vegetation patches perform quite differently from what is reported in the relevant literature. For both patch configurations B^{x}, $B^{x,ave}$ and H/h_v do not appear to be governing parameters for Manning's n on their own (Figs. 2a-c and Figs. 4a-c), and must be interpreted in conjunction with information on B^{SA}, base channel resistance, and vegetation alignment.

For example, the relationship for flow resistance proposed by V. Nikora et al. (2008) (i.e. $n = 0.025e^{3Bx,ave}$) shows good agreement with our data for both aligned and staggered alignment with $B^{SA} = 0.6$ (Fig. 4b) when a base resistance of 0.025 is used (for which we obtained exponents between $3.1B^{x,ave}$ and $3.5B^{x,ave}$). It is challenging to more thoroughly compare our results with the relevant literature since the range of $B^{x,ave}$ tested herein is limited compared to natural channels. There are also differences due to the laboratory setup with square patches of plastic grass geometrically and mechanically different from freshwater macrophytes, and with forced alignment configurations that are not natural. It is reasonable to expect that these factors influenced the absolute values of hydraulic resistance to a certain degree compared to natural vegetation. Nevertheless, the relative differences in hydraulic resistance due to different configurations should hold (or at least be representative) even if natural vegetation is considered.

In §3.1, we identified two models that perform well at predicting n for the aligned configuration: $n = 0.043(\langle R_h \rangle / h_v)^{-0.768}$ ($R^2 = 0.91$) and $n = \exp(0.437B^{SA}\text{-}2.887)\times(H/h_v)^{-0.667}$ ($R^2 = 0.92$). However, these types of models do not work as well for the staggered configuration (e.g. see the clear stratification of data in Figs. 4c and 8c-d), indicating that they probably miss fundamental mechanisms of drag production.

For prediction of hydraulic resistance, it is important to be able to account for either aligned or staggered configurations and, more in general, for the effect of patches spatial distribution. One possible approach is to use the parameter α, displayed in Fig. 6, as a correction factor that can be predicted accurately using the model reported in section 3.3, namely $\alpha = 1 + 4.04B^{SA} - 5.83(B^{SA})^2\text{-}0.09H/h_v$ ($R^2 = 0.92$). This correction factor can be used to directly account for the effects of the different flow regimes that may establish within a patch mosaic, depending on its spatial distribution, on the hydraulic resistance. For example, α incorporates the effects of preferential pathways and wake suppression. It is important to recall that α was calculated from the data using a best-fit approach. To enable the definition of a more physically-based correction factor more work is needed on the fundamental physics of flows through patch mosaics.

Bearing in mind that the values of the correction factor thus calculated are valid for the staggered configuration only (i.e. $\alpha = 1$ for aligned configuration), we expect the correction factor to assume lower values for configurations in natural ecosystems because of the presence of preferential pathways whose formation is prevented in our staggered configuration for $B^{SA} > 0.1$ (based on the trends shown in Fig. 6). In this sense, for fixed values of B^{SA} and H/h_v, a channel with a patch mosaic vegetation distribution in a staggered configuration should be characterised by the largest hydraulic resistance. Thus, we expect configurations found in natural ecosystems to perform somewhere in between aligned and staggered configurations, which define the lower and upper limit for n, respectively.

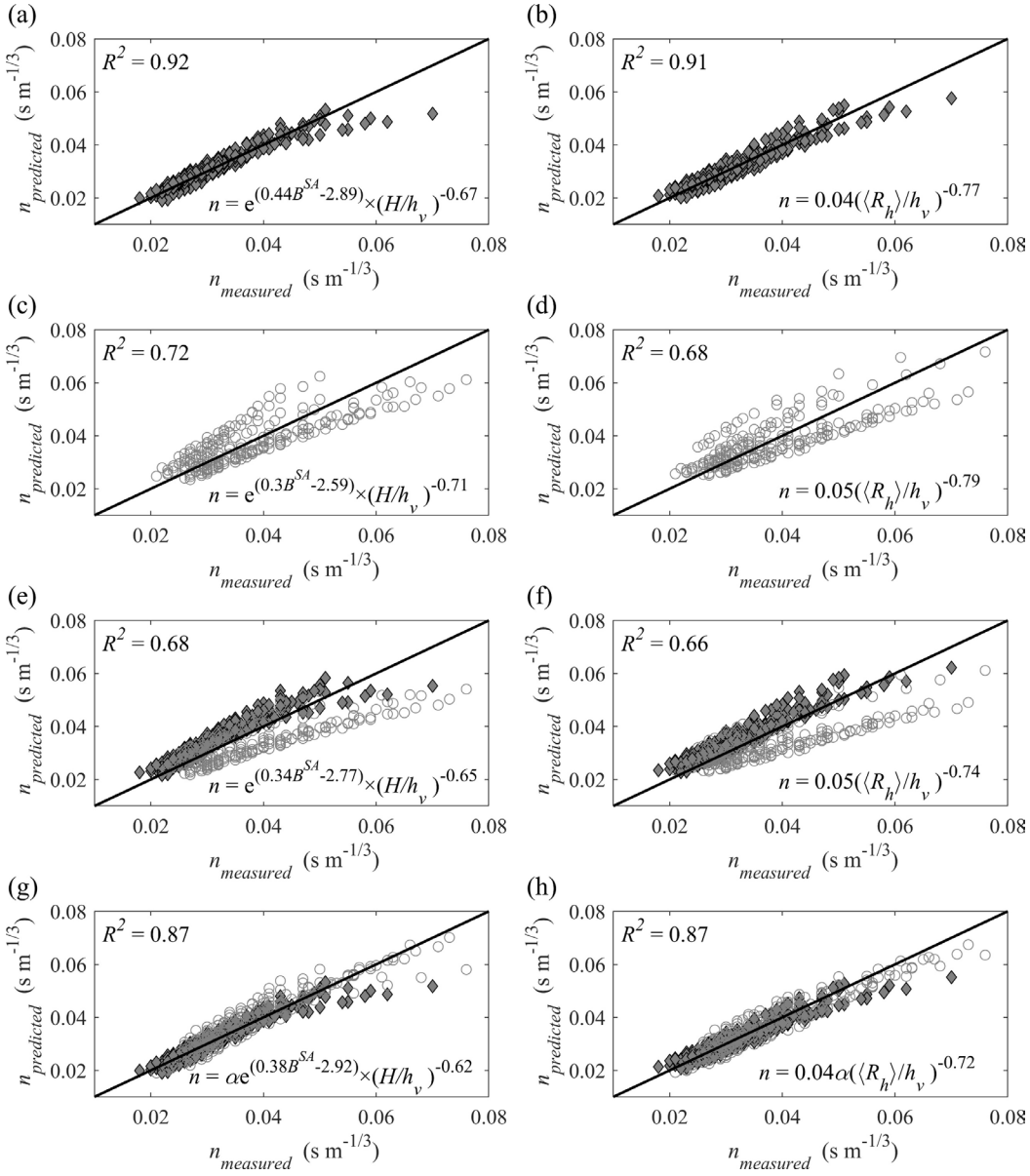

Figure 8: Measured Manning's n versus Manning's n predicted using models proposed in the paper: (a,c,e,g) multivariate regression with H/h_v and B^{SA}; (b,d,f,h) power regression with $\langle R_h \rangle / h_v$. Note that in (e-f) data are modelled with no correction factor, while in (g-h) the correction factor α is included in the models. Filled diamonds: data for aligned configurations; empty circles: data for staggered configurations. The equation and R^2 for each model are reported in the relevant plot. The solid line denotes a 1:1 agreement.

For practical applications, we introduce four additional models for Manning's n of the same forms as those introduced in sections 3.1 and 3.2 to fit all data independently of the patch configurations. With no correction for staggered cases, the best-fit relationships thus obtained are: $n = 0.05(\langle R_h \rangle / h_v)^{-0.74}$ ($R^2 = 0.66$) and $n = \exp(0.34B^{SA}-2.77) \times (H/h_v)^{-065}$ ($R^2 = 0.68$) (Fig. 8e-f). When the correction factor is used the best-fit relationships are

$n = 0.04\alpha(\langle R_h \rangle / h_v)^{-0.72}$ ($R^2 = 0.87$) and $n = \alpha\exp(0.38\mathrm{B}^{SA}\text{-}2.92)\times(H/h_v)^{-062}$ ($R^2 = 0.87$), with a notable increase in models accuracy (Fig. 8g-h). Note that models with similar accuracy are obtained if uniform cases are included in the analysis. Figure 8 displays a comparison of Manning's n predicted by the eight models introduced in this work and measured Manning's n.

All parameters considered herein to predict the hydraulic resistance through Manning's n require some knowledge of the vegetation presence across the channel. In field applications, cross-sections are characterised via measurements of vegetation height at multiple locations across each transect of interest, and many transects are required to identify a 'representative' cross-section for calculating H/h_v or B^x. This type of information enables the estimation of both the area covered by vegetation and the wetted perimeter, thus allowing for the calculation of $\langle R_h \rangle / h_v$ with no additional data. It is expected that calculating relevant parameters for the prediction of n will become easier thanks to ongoing advancements in unmanned aerial vehicles (UAVs) for aquatic vegetation monitoring. However, one should bear in mind that measurements in field settings are further complicated by the heterogeneous vertical distribution of vegetation biomass within a patch.

5. Conclusions

This paper presents the results of laboratory experiments conducted in an open channel to investigate the effect of artificial vegetation patch mosaics on hydraulic resistance. Data were collected for a range of vegetation coverages from the case of a bare bed to that of a bed fully covered by vegetation and using two spatial distributions for patches: aligned and staggered configurations. The performance of different parameters to predict Manning's n in the presence of vegetation patches was assessed for both configurations. The vegetation coverage was found to be more important at lower values of relative submergence. Manning's n for the staggered configuration (n_s) was larger than that for the aligned configuration (n_a) for all investigated cases, highlighting the importance of the spatial distribution of vegetation patches, particularly for intermediate vegetation coverage levels.

The findings of the present study indicate that the nondimensional spatially-averaged hydraulic radius performed best to predict n for the aligned configuration as an individual predictor in a relationship of the form $n \propto (\langle R_h \rangle / h_v)^{k3}$. We also identified a multivariate regression model of the form $n = \exp(c_1\mathrm{B}^{SA}\text{-}c_2)\times(H/h_v)^{c3}$ that predicts the hydraulic resistance for aligned configurations well. Further, we introduced similar models for the staggered configurations and for all data independently of the spatial configuration. Since the models do not provide very reliable results when patches are not aligned, to overcome this limitation we introduced a correction factor calculated as $\alpha = n_s/n_a$. For the case of natural vegetation

distributions in natural channels the absolute values of hydraulic resistance may vary with vegetation morphology, however, we expect the values of α found in this study (representing the effects of staggered compared to aligned patches), to be representative of natural scenarios. Detailed fieldwork with natural aquatic vegetation in different spatial configurations is recommended to assess the correspondence of α and hydraulic resistance relationships to those found in this systematic laboratory based study.

Acknowledgements

The authors gratefully acknowledge the assistance of Roy Gillanders and Benjamin Stratton for technical support during the experiments. The authors also thank the following master's students: Valentina Boscolo, Ross Kemlo, and Nico Bettio, for their help during the experiments.

Funding

The study has been supported by three EPSRC/UK grants: 'High-resolution numerical and experimental studies of turbulence-induced sediment erosion and near-bed transport' (EP/G056404/1), 'Bed friction in rough-bed free-surface flows: a theoretical framework, roughness regimes, and quantification' (EP/K041088/1) and 'Secondary currents in turbulent flows over rough walls' (EP/V002414/1).

Notation

A	=	wetted area (m^2)
B^{SA}	=	surface area blockage factor (-)
B^{x}	=	cross-sectional blockage factor (-)
$B^{x,ave}$	=	flume-averaged cross-sectional blockage factor (-)
b_x	=	length of a patch (m)
b_y	=	width of a patch (m)
B	=	flume width (m)
c_1	=	coefficient in multivariate regression model $n = \exp(c_1 B^{SA} - c_2) \times (H/h_v)^{c3}$ (-)
c_2	=	coefficient in multivariate regression model $n = \exp(c_1 B^{SA} - c_2) \times (H/h_v)^{c3}$ (-)
c_3	=	coefficient in multivariate regression model $n = \exp(c_1 B^{SA} - c_2) \times (H/h_v)^{c3}$ (-)
F_r	=	Froude number (-)
g	=	gravitational acceleration ($m\ s^{-2}$)
k_1	=	exponent in the relationship $n \propto (B^x)^{k1}$ (-)

k_2 = exponent in the relationship $n \propto (H/h_v)^{k2}$ (-)

k_3 = exponent in the relationship $n \propto (\langle R_h \rangle/h_v)^{k3}$ (-)

L = flume length (m)

h_v = mean deflected height of a patch (m)

H = mean water depth (m)

m = proportion of unvegetated cross sections along the channel (-)

n = Manning's resistance coefficient (s $m^{-1/3}$)

n_a = Manning's resistance coefficient for aligned configuration (s $m^{-1/3}$)

n_b = Manning's resistance coefficient for benchmark configuration (s $m^{-1/3}$)

n_s = Manning's resistance coefficient for staggered configuration (s $m^{-1/3}$)

N_t = total number of patches in the flume (-)

N_x = number of patches rows along the flume (-)

N_y = number of patches across a vegetated cross section (-)

$N_{y,s}$ = number of patch sides across a vegetated cross section (-)

Q = mean flow rate (L s^{-1})

$\mathsf{R_e}$ = Reynolds number (-)

R_h = hydraulic radius of unvegetated cross section (m)

$\langle R_h \rangle$ = spatially-averaged hydraulic radius (m)

$R_{h\text{-}veg}$ = hydraulic radius of vegetated cross section (m)

S = flume bed slope (-)

u_* = shear velocity (m s^{-1})

U = cross sectional mean velocity (m s^{-1})

α = correction factor for Manning's n (-)

Δx = patch spacing in the x direction (m)

Δy = patch spacing in the y direction (m)

ν = water kinematic viscosity (m^2 s^{-1})

φ = porosity (-)

References

Afzalimehr, H., Riazi, P., Jahadi, M., & Singh, V. P. (2021). Effect of vegetation patches on flow structures and the estimation of friction factor. *ISH Journal of Hydraulic Engineering*, *27*(sup1), 390–400.

Albayrak, I., Nikora, V., Miler, O., & O'Hare, M. (2012). Flow-plant interactions at a leaf scale: Effects of leaf shape, serration, roughness and flexural rigidity. *Aquatic Sciences*, *74*(2), 267–286. https://doi.org/10.1007/s00027-011-0220-9

Arcement, G. J., & Schneider, V. R. (1989). *Guide for selecting Manning's roughness*

coefficients for natural channels and flood plains. US Government Printing Office Washington, DC.

Bal, K., Struyf, E., Vereecken, H., Viaene, P., De Doncker, L., de Deckere, E., Mostaert, F., & Meire, P. (2011). How do macrophyte distribution patterns affect hydraulic resistances? *Ecological Engineering*, *37*(3), 529–533.

Barnes, H. H. (1967). *Roughness characteristics of natural channels* (Issue 1849). US Government Printing Office.

Biggs, H. J. (2020). Aquatic Vegetation Monitoring with UAS. In *Unmanned Aerial Remote Sensing* (pp. 35–53). CRC Press.

Biggs, H. J., Haddadchi, A., & Hicks, D. M. (2021). Interactions between aquatic vegetation, hydraulics and fine sediment: A case study in the Halswell River, New Zealand. *Hydrological Processes*, *35*(6), e14245.

Biggs, H. J., Nikora, V., Gibbins, C. N., Fraser, S., Green, D. R., Papadopoulos, K., & Hicks, D. M. (2018). Coupling Unmanned Aerial Vehicle (UAV) and hydraulic surveys to study the geometry and spatial distribution of aquatic macrophytes. *Journal of Ecohydraulics*, *3*(1), 1–14. https://doi.org/10.1080/24705357.2018.1466666

Biggs, H. J., Nikora, V. I., Gibbins, C. N., Cameron, S. M., Papadopoulos, K., Stewart, M., Fraser, S., Vettori, D., Savio, M., & O'Hare, M. T. (2019). Flow interactions with an aquatic macrophyte: a field study using stereoscopic particle image velocimetry. *Journal of Ecohydraulics*, *4*(2), 113–130.

Butcher, R. W. (1933). Studies on the ecology of rivers: I. On the distribution of macrophytic vegetation in the rivers of Britain. *The Journal of Ecology*, 58–91.

Champion, P. D., & Tanner, C. C. (2000). Seasonality of macrophytes and interaction with flow in a New Zealand lowland stream. *Hydrobiologia*, *441*, 1–12.

Chang, K., & Constantinescu, G. (2015). Numerical investigation of flow and turbulence structure through and around a circular array of rigid cylinders. *Journal of Fluid Mechanics*, *776*, 161–199. https://doi.org/10.1017/jfm.2015.321

Chow, V. T. (1959). Open-channel hydraulics. *McGraw-Hill Civil Engineering Series*.

Cornacchia, L., Licci, S., Nepf, H. M., Folkard, A. M., van der Wal, D., van de Koppel, J., Puijalon, S., & Bouma, T. J. (2019). Turbulence-mediated facilitation of resource uptake in patchy stream macrophytes. *Limnology and Oceanography*, *64*(2), 714–727. https://doi.org/10.1002/lno.11070

Cowan, W. L. (1956). Estimating hydraulic roughness coefficients. *Agricultural Engineering*, *37*(7), 473–475.

Figueiredo, B. R. S., Mormul, R. P., & Thomaz, S. M. (2015). Swimming and hiding regardless of the habitat: prey fish do not choose between a native and a non-native macrophyte species as a refuge. *Hydrobiologia*, *746*(1), 285–290.

Folkard, A. M. (2011). Flow regimes in gaps within stands of flexible vegetation: Laboratory flume simulations. *Environmental Fluid Mechanics*, *11*(3), 289–306. https://doi.org/10.1007/s10652-010-9197-5

Green, J. C. (2005). Comparison of blockage factors in modelling the resistance of channels containing submerged macrophytes. *River Research and Applications*, *21*, 671–686. https://doi.org/10.1002/rra.854

Green, J. C. (2006). Effect of macrophyte spatial variability on channel resistance. *Advances in Water Resources*, *29*, 426–438. https://doi.org/10.1016/j.advwatres.2005.05.010

Gurnell, A. M., Van Oosterhout, M. P., De Vlieger, B., & Goodson, J. M. (2006). Reach-scale interactions between aquatic plants and physical habitat: River Frome, Dorset. *River Research and Applications*, *22*(6), 667–680.

Hicks, D. M., & Mason, P. D. (1998). *Roughness characteristics of New Zealand rivers: National Institute of Water and Atmospheric Research Ltd*. Water Resources Publications, LLC.

Husson, E., Hagner, O., & Ecke, F. (2014). Unmanned aircraft systems help to map aquatic vegetation. *Applied Vegetation Science*, *17*(3), 567–577.

Kouwen, N., & Unny, T. E. (1973). Flexible roughness in open channels. *Journal of the Hydraulics Division*, *HY5*, 713–729.

Kouwen, N., Unny, T. E., & Hill, H. M. (1969). Flow retardance in vegetated channels. *Journal of the Irrigation and Drainage Division*, *IR2*, 329–342.

Larsen, L. G., Ma, J., & Kaplan, D. (2017). How important is connectivity for surface water fluxes? A generalized expression for flow through heterogeneous landscapes. *Geophysical Research Letters*, *44*(20), 10–349.

Lee, B. E., & Soliman, B. F. (1977). An investigation of the forces on three dimensional bluff bodies in rough wall turbulent boundary layers. *Journal of Fluids Engineering*, *99*(3), 503–509.

Leonardi, S., Orlandi, P., & Antonia, R. A. (2007). Properties of d-and k-type roughness in a turbulent channel flow. *Physics of Fluids*, *19*(12), 125101.

Luhar, M., & Nepf, H. M. (2011). Flow-induced reconfiguration of buoyant and flexible aquatic vegetation. *Limnology and Oceanography*, *56*(6), 2003–2017. https://doi.org/10.4319/lo.2011.56.6.2003

Luhar, M., & Nepf, H. M. (2013). From the blade scale to the reach scale: A characterization of aquatic vegetative drag. *Advances in Water Resources*, *51*, 305–316. https://doi.org/10.1016/j.advwatres.2012.02.002

Morris, H. M. (1955). Flow in rough conduits. *Transactions of the American Society of Civil Engineers*, *120*(1), 373–398.

Nepf, H. M. (2012). Hydrodynamics of vegetated channels Hydrodynamics of vegetated

channels. *Journal of Hydraulic Research*, *50*(3), 262–279.

Nikora, N., Nikora, V., & O'Donoghue, T. (2013). Velocity profiles in vegetated open-channel flows: combined effects of multiple mechanisms. *Journal of Hydraulic Engineering*, *139*(10), 1021–1032.

Nikora, V., Larned, S., Nikora, N., Debnath, K., Cooper, G., & Reid, M. (2008). Hydraulic Resistance due to Aquatic Vegetation in Small Streams : Field Study. *Journal of Hydraulic Engineering*, *134*(9), 1326–1332.

Savio, M. (2017). *Turbulent structure and transport processes in open-channel flows with patchy-vegetated beds* [University of Aberdeen]. https://abdn.alma.exlibrisgroup.com/discovery/delivery/44ABE_INST:44ABE_VU1/12152788030005941

Siniscalchi, F., & Nikora, V. (2012). Flow-plant interactions in open-channel flows: A comparative analysis of five freshwater plant species. *Water Resources Research*, *48*(5), 1–13. https://doi.org/10.1029/2011WR011557

Siniscalchi, F., Nikora, V., & Aberle, J. (2012). Plant patch hydrodynamics in streams: Mean flow, turbulence, and drag forces. *Water Resources Research*, *48*(1), 1–14. https://doi.org/10.1029/2011WR011050

Taddei, S., Manes, C., & Ganapathisubramani, B. (2016). Characterisation of drag and wake properties of canopy patches immersed in turbulent boundary layers. *Journal of Fluid Mechanics*, *798*, 27–49. https://doi.org/10.1017/jfm.2016.312

Vettori, D., Niewerth, S., Aberle, J., & Rice, S. P. (2021). A link between plant stress and hydrodynamics? Indications from a freshwater macrophyte. *Water Resources Research*, *57*(9), e2021WR029618.

Wolfe, S. A., & Nickling, W. G. (1993). The protective role of sparse vegetation in wind erosion. *Progress in Physical Geography*, *17*(1), 50–68.

Wright, K., Hiatt, M., & Passalacqua, P. (2018). Hydrological connectivity in vegetated river deltas: The importance of patchiness below a threshold. *Geophysical Research Letters*, *45*(19), 10–416.

Zampiron, A., Nikora, V., Cameron, S., Patella, W., Valentini, I., & Stewart, M. (2020). Effects of Streamwise Ridges on Hydraulic Resistance in Open-Channel Flows. *Journal of Hydraulic Engineering*, *146*(1), 6019018.

List of tables

List of figures